CHEMISTRY OF MATERIALS

Article

pubs.acs.org/cm

Water Sorption Cycle Measurements on Functionalized MIL-101Cr for Heat Transformation Application

Anupam Khutia,[†] Holger Urs Rammelberg,[‡] Thomas Schmidt,*[,‡] Stefan Henninger,[§] and Christoph Janiak*[,†]

[†]Institut für Anorganische Chemie und Strukturchemie, Universität Düsseldorf, Universitätsstraße 1, D-40225 Düsseldorf, Germany

[‡]Leuphana Universität Lüneburg, Institut für Umweltchemie, Scharnhorststraße, D-21335 Lüneburg, Germany

[§]Department of Thermally Active Materials and Solar Cooling, Fraunhofer Institute for Solar Energy Systems ISE, Heidenhofstraße 2, 79110 Freiburg, Germany

Supporting Information

ABSTRACT: The water loading capacity and water cycle stability (40 adsorption/desorption cycles) of four nitro- or amino-functionalized MIL-101Cr materials (**1**–**4**) is assessed for heat transformation applications. Amino- or nitro-functionalized (**1**, **3**) and partially amino- or nitro-functionalized MIL-101Cr (**2**, **4**) have been synthesized through time-controlled postsynthetic modification of MIL-101Cr. The partially functionalized materials (**2**, **4**) contain about 78 mol % amino- or nitro-functionalized terephthalate linker. Hydrophilic nitro or amino functionalities were introduced into MIL-101Cr in order to achieve water loading at lower p/p_0 values for possible use in thermally driven adsorption chillers or heat pumps. Among the four materials studied, fully aminated MIL-101Cr-NH_2, **1**, and partially aminated MIL-101Cr-pNH_2, **2**, showed the best water loadings (about 1.0 gH_2O/gMIL) as well as water stability over 40 adsorption–desorption cycles. After 40 cycles, the X-ray powder diffractogram and Brunauer–Emmett–Teller (BET) surface determination of amino-functionalized materials indicated structural integrity with Δ_{BET} = −6.3% after 40 cycles, while the nitro-functionalized MIL-101Cr exhibited a decrease in their BET surface of Δ_{BET} = −25% and −20% for **3** and **4**, respectively.

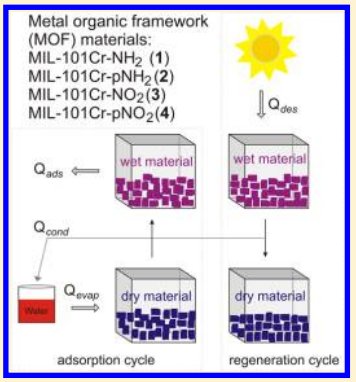

KEYWORDS: *water sorption, metal–organic frameworks, MIL-101Cr, postsynthetic modification, heat transformation*

INTRODUCTION

In recent years, research on thermally driven adsorption chillers (TDCs) or adsorption heat pumps (AHPs) has gained increasing attention for low-temperature heat transformation applications.[1,2] Traditional compression cooling systems or air conditioning devices use electrical energy, thereby significantly contributing to CO_2 emission. The demand of electrical energy for air conditioning is expected to increase rapidly in the future due to higher living standards as well as architectural trends. To counteract this development, energy-saving air-conditioning technologies are urgently needed. The use of low-temperature waste heat from industrial processes or even solar energy in TDCs provide a promising approach toward heating or cooling with alternative technologies.

Though several working principles are known for this purpose, the reversible evaporation and subsequent adsorption of a working fluid has proven most promising. The principle of this method is illustrated in Figure 1. In the production or adsorption cycle, a working fluid is evaporated, taking evaporation heat Q_{evap}, thereby producing useful cold in the cooling case, or heat is extracted from a low-temperature heat source in a heating application. Then vapor of the working fluid is adsorbed into a porous material, generating adsorption heat Q_{ads}. This heat is released to the environment in the cooling case or it produces useful heat in the heat pump application. In the regeneration cycle, the porous material is regenerated by applying driving heat Q_{des} for desorption from various external sources like solar energy, industrial waste heat, or a gas burner. The adsorbed fluid that is released condenses at a medium temperature level, releasing the heat of condensation Q_{cond}. This is useful in the heat pump and is released to the environment in cooling application.

Mostly water is used as the working fluid because of its high evaporation enthalpy and ready availability, though other solvents can also be employed for this process. Various adsorbent (solid material)–adsorbate (working fluid) pairs, for example, zeolite–water, silica gel–water, active carbon–methanol, and active carbon–ammonia, have been studied for these purposes.[3] Though silica gel and zeolites are currently employed in commercial applications, they have many disadvantages.[4,5] Zeolites have a high affinity for water and already adsorb at low relative pressure of p/p_0 0.001–0.01, but they require high desorption temperatures (typically over 300 °C) and have a low water loading. Silica gels have less

Received: December 19, 2012
Revised: February 8, 2013
Published: February 11, 2013

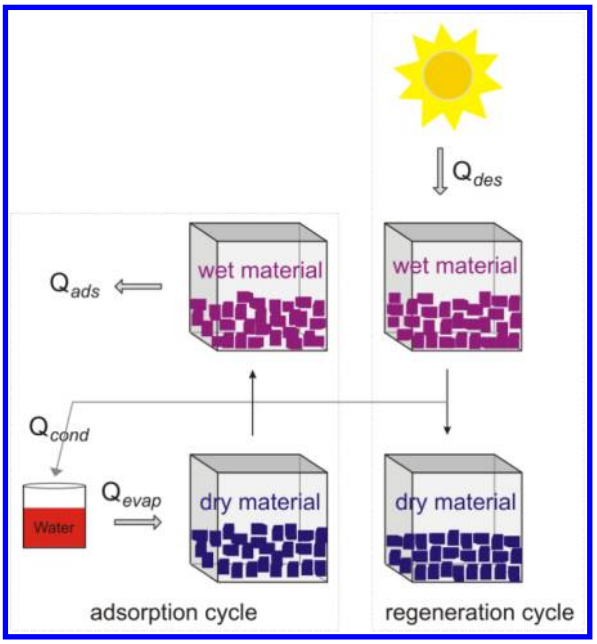

Figure 1. Working principle in a thermally driven adsorption heat pump or cooler showing adsorption and regeneration cycle.

hydrophilic character than zeolites, which leads to lower desorption temperatures (typically ca. 100 °C) but also to low water exchange within a cycle. Therefore, further development is required on porous materials, which should show a sudden uptake of water vapor at low to medium humidity and also desorption of water vapor from the material at low temperature (below 80 °C).[6] For ideal performance, a porous material should perform in the $0.05 < p/p_0 < 0.4$ relative pressure range and should have a desorption temperature at or below 80 °C.[7,8]

Metal organic frameworks (MOFs)/porous coordination polymers (PCPs)[9] have attracted tremendous attention over the past years.[10] This is due to their porosity, large inner surface area, tunable pore sizes, and topologies, which leads to versatile architectures and promising applications, such as ion exchange; gas adsorption and storage of, in particular, hydrogen and methane;[11] gas[12] and liquid[13] separation processes;[14] drug delivery;[15] sensor technology;[16] heterogeneous catalysis;[17] hosts for metal colloids or nanoparticles[18] or polymerization reactions;[19] luminescence;[20] nonlinear optics;[21] pollutant sequestration;[22] and magnetism.[23]

PCPs/MOFs are well-known porous materials owing to extremely high possible surface areas (>6000 m^2/g in the case of MOF-210[24] or NU-100[25]), exceeding the values for silica gels, active carbons, and zeolites. Compared with other sorption or porous materials like active carbon or zeolites, the sorption properties of MOFs can be designed and fine-tuned through the organic ligands, including their postsynthetic modification.[26] Variation of the organic ligand's functionality provides ample opportunities for pore size tuning and for changing the affinity of the surface toward different adsorbates. An advantage of MOFs over other porous materials is their perfectly identical pore size over the whole framework structure.

The hydrothermal instability of most MOFs limits their industrial application as adsorbents. However, MOFs that are synthesized hydrothermally are expected to show higher water stability, though their porosity as well as crystallinity in the absence of water molecules needs to be explored. The research group of Férey[27,28] has hydrothermally synthesized a series of porous materials, also known as MILs (MIL stands for Material Institute Lavoisier). These materials have high surface areas and large pore volumes. Work on MOFs as water adsorbents is gaining attention since an early report by Aristov[1d] and a report of water adsorption on ISE-1 from our group.[29] MIL-type materials adsorb huge amounts of water (1.0−1.5 g/g for MIL-101Cr,[7,30,31] 0.6−0.7 g/g for MIL-100Cr,[32] 0.65−0.75 g/g for MIL-100Fe,[31,33] and 0.5 g/g for MIL-100Al[33]) and have very good water cycle stability.

MIL-101Cr, with the empirical formula $[Cr_3(O)(BDC)_3(F,OH)(H_2O)_2]$ (where BDC = benzene-1,4-dicarboxylate) is a chromium−terephthalate-based porous material. Its structure resembles the augmented MTN zeolite topology. MIL-101Cr has two types of inner cages with diameters of 29 and 34 Å and pore aperture windows diameter of up to 16 Å (Figure 2) with high surface area (BET surface area of 4000

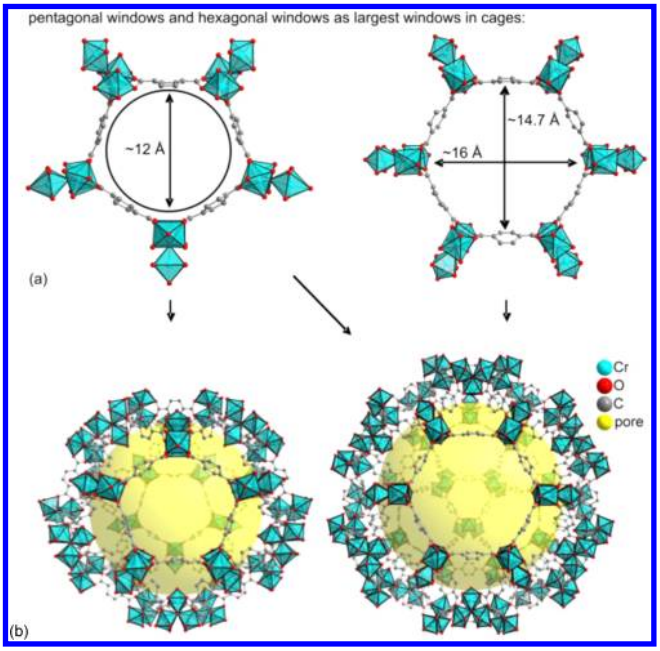

Figure 2. Building blocks for MIL-101Cr, $[Cr_3(O)(BDC)_3(F,OH)(H_2O)_2]$. The benzene-1,4-dicarboxylate ligands bridge between trinuclear $\{Cr_3O\}$ building units. The largest aperture windows (a) of the mesoporous cages (b), which build up the MTN zeolite network, are pentagonal and hexagonal rings. The yellow spheres in the mesoporous cages in panel b, with radii of 14.5 or 17 Å, respectively, take into account the van der Waals radii of the framework walls (water-guest molecules are not shown; adapted from CSD-Refcode OCUNAK).[34].

m^2/g).[34] MIL-101Cr is synthesized in quite harsh reaction conditions (220 °C in water). Thus, a fundamental water stability of this material can be expected, which was explored before from our research group.[30] MIL-101Cr adsorbs most water in the relative pressure range $0.40 < p/p_0 < 0.54$.[30] Although the results are very promising, MIL-101Cr could not meet the criteria for ideal performance in heat transformation applications.

In order to improve the water sorption performance of MIL-101Cr, we have introduced hydrophilic nitro ($-NO_2$) and amino functionality ($-NH_2$) via postsynthetic modification (PSM). PSM is now a widely used technique to create suitable functionality in the organic linkers in MOFs.[35] Nitro and amino functional groups were introduced in MIL-101Cr under

dx.doi.org/10.1021/cm304055k | Chem. Mater. 2013, 25, 790−798

extremely strong acidic conditions (nitrating acid for nitration and $SnCl_2$/concentrated HCl for amination, cf. Scheme 1).[36]

Scheme 1. Schematic Synthetic Routes for Postsynthetic Modification of MIL-101Cr to MIL-101Cr-(p)NO_2 and MIL-101Cr-(p)NH_2[a]

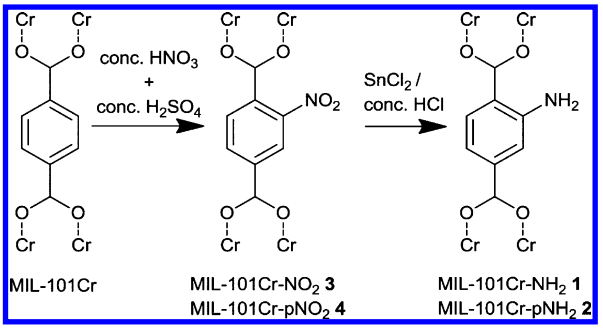

[a]p = partial.

Moreover, partially functionalized materials (-pNO_2 and -pNH_2) with two different organic ligands in the same framework have been synthesized, which are difficult to obtain through direct synthesis. Recently a water sorption study of functional MIL-101Cr materials was reported in the literature.[37] Yet our work on functionalized MIL-101Cr differs: we have explored the water sorption properties of MIL-101Cr-NH_2 (**1**), MIL-101Cr-pNH_2 (**2**), MIL-101Cr-NO_2 (**3**), and MIL-101Cr-pNO_2 (**4**), where p stands for partial ligand amination and nitration; that is, functionalized MIL-101Cr materials containing two different ligands. Water loadings and water stabilities of these modified MIL-101Cr materials have been examined over 40 sorption cycles together with desorption kinetics. This study of hydrothermal cycle stability is a valuable factor for determining applications in a real environment.

RESULTS AND DISCUSSION

MIL-101Cr batches were prepared hydrothermally from chromium nitrate and terephthalic acid as reported in the literature.[34] The as-synthesized materials were activated through washing with *N*,*N*-dimethylformamide (DMF), methanol, and water (see Supporting Information). The postsynthetic modification of MIL-101Cr followed the route of nitration by use of mixed nitrating acid (concentrated HNO_3/concentrated H_2SO_4) to yield MIL-101Cr-NO_2 (**3**) and subsequent reduction by $SnCl_2$/concentrated HCl to obtain MIL-101Cr-NH_2 (**1**) (Scheme 1) (see Supporting Information).[36]

Nitration of the MIL-101Cr sample with a short defined reaction time reproducibly leads to the formation of MIL-101Cr samples containing incompletely (78 mol %) nitrated organic linkers, which means it produces mixed-ligand MIL-101Cr samples containing both terephthalate and 2-nitroterephthalate (molar ratio ~1:3.6). This approach opens a new possibility toward the synthesis of mixed-ligand porous materials. Hydrothermal synthesis of two organic ligands simultaneously with the same metal cluster can produce a mixture of materials composed of either individual ligands or mixed ligands, which are very difficult to separate from each other. However, the above time-controlled postsynthetic modification method can exclusively lead to formation of mixed-ligand material. In this way two mixed-ligand MIL-101Cr samples, namely, MIL-101Cr-pNO_2 (**4**) and MIL-101Cr-pNH_2 (**2**), were prepared (see Supporting Information for detailed synthesis and activation procedure). The ratio of ligands was determined after decomposition of a probe from the functionalized MIL-101Cr samples with aqueous NaOH solution (see Supporting Information). The mixed ligand complexes **2** and **4** reproducibly contain about 78 mol % 2-aminoterephthalato and 2-nitroterephthalato ligand, respectively, as determined from the relative intensities of the individual signals in ^{1}H NMR spectra (Figure 3). All modified MIL-101Cr samples were

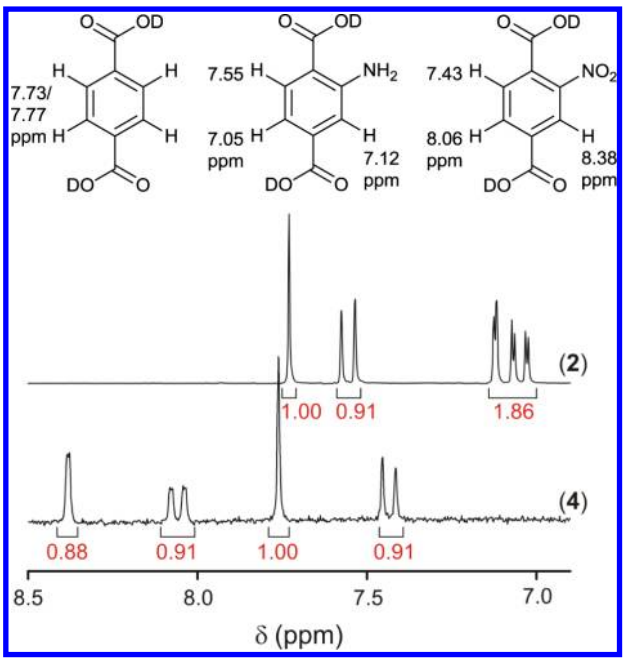

Figure 3. Example of ^{1}H NMR spectra (200 MHz) of the organic linkers in D_2O/NaOD solution after decomposition of partially aminated/nitrated MIL-101Cr-pNH_2/NO_2 (**2**/**4**, respectively), with the relative intensities and assignments of individual (pH-dependent) resonances.

characterized by powder X-ray diffractometry (PXRD) and Brunauer–Emmett–Teller (BET) surface area analysis. PXRD patterns of MIL-101Cr samples match well with the simulated MIL-101Cr pattern (Figure 4), which confirms that the original MIL-101 framework was retained in all modified samples. BET surface areas of each sample were measured from N_2 sorption isotherms (Table 1). MIL-101Cr-NH_2 (**1**) has the highest BET surface area as well as total and micropore volume among all four modified materials. MOFs are microporous materials, so over 80–90% of the pore volume is present as micropore volume (Table 1).

Water Sorption Isotherms. Water sorption isotherms (Figure 5) of the four postsynthetically modified MIL-101Cr samples were measured volumetrically to examine the effect of ligand functionality. The characteristics of the water adsorption isotherms of MIL-101Cr-NH_2 (**1**) and MIL-101Cr-NO_2 (**3**) are in good agreement with previously reported results.[37] MIL-101Cr-NH_2 adsorbs a comparable amount of water, but MIL-101Cr-NO_2 showed less water sorption compared to previously reported results (0.44 g of H_2O in **3** versus 0.90 g of H_2O/g of dry sorbent in ref 37). This can be attributed to the difference in BET surface area and pore volume of the material (Table 1 and ref 37). Similar incidents were found with MIL-101Cr, which is known to adsorb 1.0–1.5 g/g water depending on accessible surface area.[7,30,31]

dx.doi.org/10.1021/cm304055k | *Chem. Mater.* 2013, 25, 790–798

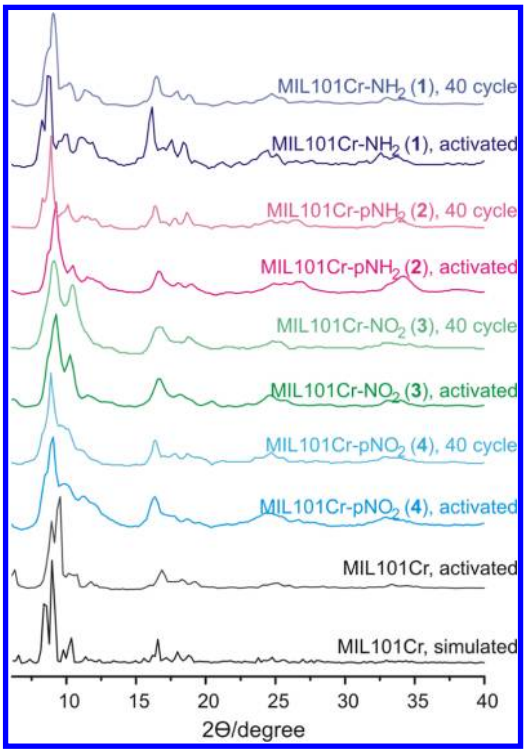

Figure 4. PXRD patterns of functionalized MIL-101Cr samples **1**–**4**.

At high humidity (p/p_0 = 0.8–0.9) the water adsorption correlates with the available pore volume, but it is not the only factor. In addition, hydrophobicity/hydrophilicity of the ligand, hydrogen-bonding capabilities, directing and interference effects of functional groups, site preference, and possible degradation or structure transition of the material can be important influential factors for water uptake capacity, as was discussed for functionalized Zr-based UiO-66 MOFs.[38]

Like MIL-101Cr, all modified samples showed a small amount of water adsorption even at small relative pressure (p/p_0 < 0.35) due to water coordination and cluster formation at the hydrophilic vacant metal sites. Significant adsorption of water occurred in a stepwise manner with consecutive filling of the two different mesopores of 29 and 34 Å (see also Figures S6–S9 in Supporting Information). Compared to the non-modified MIL-101Cr material, the amino-functionalized compounds **1** and **2** start to show large water uptake already below $p/p_0 \approx 0.4$ (Figure 5, bottom right), in agreement with their anticipated increased hydrophilicity through the added hydrophilic amino sites.[37] In addition, marked differences were observed among the adsorption isotherms of the modified samples in this pore filling region. Amino-functionalized compounds (**1** and **2**) adsorb water within a narrow range of 0.38 < p/p_0 < 0.48. However, water adsorption isotherms in nitro-functionalized **3** and **4** were widely dispersed and showed an increased hysteresis at p/p_0 0.35–0.65. Water loadings were also markedly different for amino- and nitro-functionalized materials (1.06 g/g for **1**, 0.44 g/g for **3**; see Table 1). In order to explain the large water uptake of **1** and **2**, we have measured the nitrogen sorption isotherms of all postsynthetically modified materials (**1**–**4**) at 77 K. The BET surfaces and total micropore volumes of **1** and **2** are much higher than those of **3** and **4** (Table 1). This explains the larger water uptake capacity of the amino- over the nitro-functionalized materials. All the materials showed a distinct hysteresis between adsorption and desorption branches widely known for mesoporous materials.[7,30,33] Unfortunately, this hysteresis somewhat reduces the usable part of the loading lift of the materials.

Heat of Adsorption. Heat of adsorption is an important parameter in adsorption chillers or heat pumps, because it is either useful heat or released to the environment depending on the direction of operation. The differential heat of adsorption can be calculated by use of the Clausius–Clapeyron equation (eq 1)[39] from water adsorption isotherms at 293 and 303 K; see Figures S10 and S11 in Supporting Information.

$$\Delta H_{\mathrm{ads,diff}} = -R \ln\left(\frac{p_2}{p_1}\right)\frac{T_1 T_2}{T_2 - T_2} \qquad (1)$$

The obtained average heat of adsorption values for **1**–**4** (Table 2) are slightly above the molar enthalpy of condensation for water (40.7 kJ/mol).

When these values for heat of adsorption are compared with those for zeolites (Na-A, Li-LSX, and silica-aluminophosphate, SAPOs) or aluminophosphates (AlPOs), distinct differences can be noted.[5] The adsorption enthalpy for zeolites is very high at low adsorbed mass and then gradually decreases, similar to MIL materials. However, the average heat of adsorption in zeolites is still higher (Table 2) which clearly indicates the presence of strong host–guest interactions.

Water Cycle Stability. In order to evaluate hydrothermal stability, materials **1**–**4** were exposed to continuous water adsorption and desorption cycle experiment between 40 and

Table 1. Nitrogen and Water Adsorption Measurements before and after 40 Water Sorption Cycles

	before 40 cycles			after 40 cycles					
compds	BET surface area[a] (m^2/g)	micropore volume[b] (cm^3/g)	total pore volume[c] (cm^3/g)	BET surface area[a] (m^2/g)	micropore volume[b] (cm^3/g)	total pore volume[c] (cm^3/g)	Δ_{BET} (%)	$\Delta_{\text{total pore volume}}$ (%)	max. water loading[d] (g/g at 20 °C)
MIL-101Cr-NH_2 (**1**)	2690	1.44	1.60	2520	1.36	1.54	−6.3	−3.7	1.06
MIL-101Cr-pNH_2 (**2**)	2495	1.33	1.44	2340	1.31	1.49	−6.3	+3.5	1.05
MIL-101Cr-NO_2 (**3**)	1245	0.58	0.70	930	0.45	0.58	−25.3	−17.6	0.44
MIL-101Cr-pNO_2 (**4**)	2195	1.03	1.11	1760	0.91	0.97	−20	−12.6	0.60

[a]BET surface area of activated material was calculated at 0.05 < p/p_0 < 0.2 from N_2 sorption isotherm at 77 K with a standard deviation of ±50 m^2/g. [b]Calculated from N_2 sorption isotherm at 77 K (p/p_0 = 0.5) for pores ≤2 nm. [c]Calculated from N_2 sorption isotherm at 77 K (p/p_0 = 0.95) for pores ≤20 nm. [d]Calculated from water sorption isotherm at 293 K (p/p_0 = 0.9) before water sorption cycles.

dx.doi.org/10.1021/cm304055k | Chem. Mater. 2013, 25, 790–798

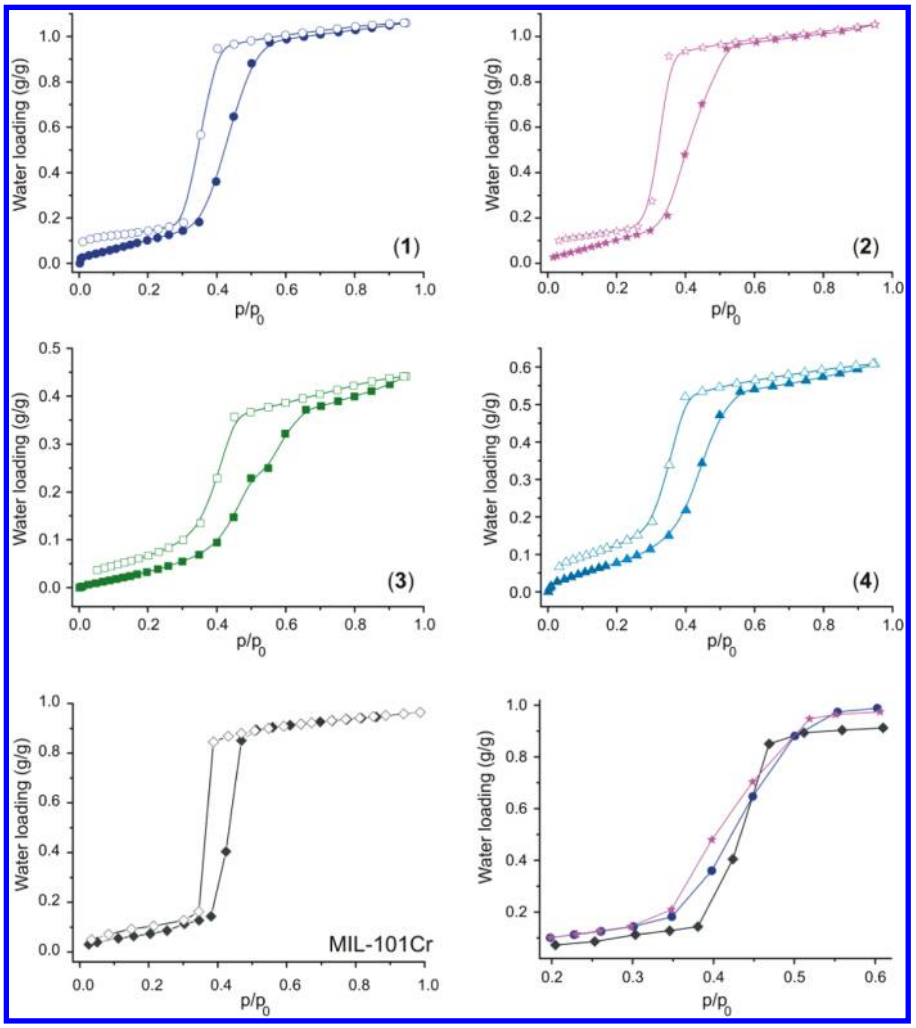

Figure 5. Water sorption isotherms of postsynthetically modified MIL-101Cr samples at 20 °C: MIL-101Cr-NH_2 (**1**); MIL-101Cr-pNH_2 (**2**); MIL-101Cr-NO_2 (**3**); MIL-101Cr-pNO_2 (**4**). Also shown is the water sorption isotherm of nonmodified MIL-101Cr (bottom left) and an overlay of the enlarged adsorption isotherms of MIL-101Cr together with **1** and **2** (bottom right). Closed and open symbols refer to adsorption and desorption, respectively.

Table 2. Adsorption Enthalpy of Water for Various Porous Materials

compd	avg heat of adsorption (kJ/mol)	ref
Na-A	57	2e
Li-LSX (low silica X)	58	2e
SAPO-34	55−57	2b, e
AlPO-18	55	2b, e
MIL-101Cr-NH_2 (**1**)	43	this work[a]
MIL-101Cr-pNH_2 (**2**)	43	this work[a]
MIL-101Cr-NO_2 (**3**)	46	this work[a]
MIL-101Cr-pNO_2 (**4**)	48	this work[a]
MIL-101Cr	45	31
MIL-100Fe	49	31, 33
MIL-100Al	44	33

[a]Figures S10 and S11 in Supporting Information.

140 °C under a water vapor pressure of 5.2 kPa. The exchanged mass of water was followed over 40 repeated desorption and adsorption cycles for each compound (Figure 6 and Figures S12−S15 in Supporting Information). Compounds **1**, **3**, and **4** exhibit an initial drop in the exchanged amount of water. However, from the fourth and 15th cycle on, the desorbed and adsorbed mass of water remains constant for compounds **1** and **3**, respectively. For compound **4**, the water mass continuously decreases over 40 cycles. Only the partially aminated compound **2** shows a stable mass difference from the very beginning.

For compound **1**, the desorbed and adsorbed amount of water varies in a small range only, especially after the fourth cycle. The maximum adsorbed water mass decreased by 16%, from 0.56 g/g to 0.47 g/g over 40 cycles (see Figure S12, Supporting Information). The desorption minimum stayed essentially constant at 17.74 ± 0.03 mg. For compound **2**, the desorbed and adsorbed amount of water varied even less around an average value of 0.55 ± 0.01 g/g, whereby the desorption minimum was at 7.37 ± 0.04 mg (Figure S13, Supporting Information). For compounds **3** and **4**, a decrease in the amount of adsorbed water of 11% and 48% was observed.

We have also carried out powder X-ray diffraction (PXRD) as well as BET surface and pore analytics by nitrogen adsorption of compounds **1**−**4** after 40 water sorption cycles. There is no significant change in crystallinity of the materials as indicated by the PXRD measurements included in Figure 4. Also, amino-functionalized compounds (**1** and **2**) have almost no change in BET surface area and pore volume after 40 cycle

dx.doi.org/10.1021/cm304055k | *Chem. Mater.* 2013, 25, 790−798

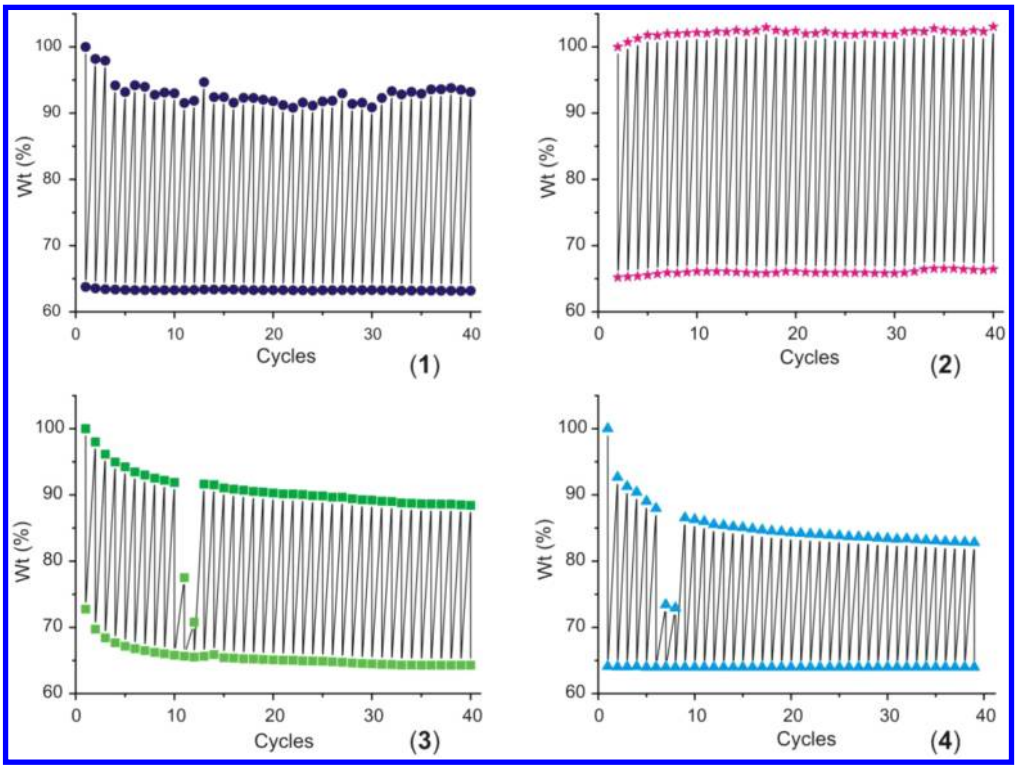

Figure 6. Change of total mass variation in compounds **1**–**4** during water desorption and adsorption over 40 cycles. The initial adsorbed water mass m_0 is set to 100% and the subsequent masses are related thereupon as m/m_0 (× 100). Outliers of the mass variation of **3** and **4** originate from intermediate regulation errors of the water vapor pressure.

as observed from N_2 sorption isotherms at 77 K (see Table 1). However, significant changes in surface area and pore volume are detected in nitro-functionalized **3** and **4** after cycle measurements. We suggest that the electron-withdrawing effect of the nitro group increases the ionic character of the Cr–carboxylate bonds and, thereby, makes it more prone to hydration and labile. These results also suggest that compounds **3** and **4** are not suitable materials for the intended application of heat transformation by water sorption over a long period of time.

Desorption Enthalpy and Kinetics. Simultaneously with the mass change, we have also determined the desorption enthalpies, which were normalized to the mass of the respective adsorbent masses (Figure 7 and Figures S16–19 in Supporting Information). The decreasing trend for compounds **1**, **3**, and **4** are in accordance with the difference between the charged and discharged state in Figure 6. For compound **2**, an increase of the normalized desorption enthalpy was observed with increasing cycle number, which can also be found in the relative difference between charged and discharged state in Figure 6.

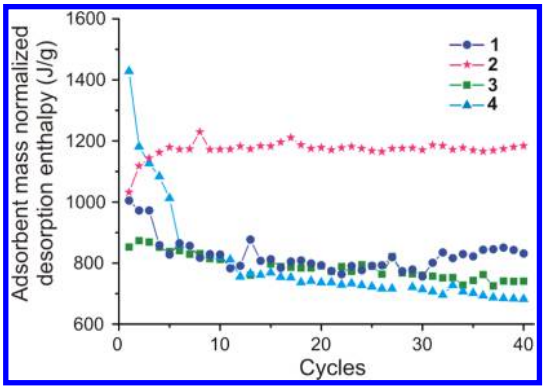

Figure 7. Adsorbent mass normalized desorption enthalpies for water desorption over 40 cycles in compounds **1**–**4**. Data points originating from the outliers for **3** and **4** in Figure 6 are not shown.

For the interesting amino-functionalized compounds **1** and **2**, we obtained kinetic desorption data by following the water removal in the thermogravimetric analysis (TGA) at different heating rates. Figure 8 shows the desorption kinetics of **1** and **2** with heating rates of 0.1, 1, and 10 K/min. Desorption is delayed for higher heating rates of 10 and 1 K/min compared to 0.1 K/min, as expected. At a heating rate of 0.1 K/min, the water desorption is almost finished at a temperature of 55 °C. For a heating rate of 1 K/min, the water desorption is delayed up to 70–80 °C, and for a heating rate of 10 K/min, the delay extends to 120 °C and above. While at 10 K/min a sigmoidal desorption curve is observed, a deviation from the "classical" sigmoidal course is found for 0.1 K/min and (less obviously) for 1 K/min. Instead, the course of the kinetic curves of **1** and **2** at 0.1 K/min can be described by a combination of two sigmoidal curves. This phenomenon indicates different coordination sites with different activation barriers. We conclude that, for **1** and **2**, the interactions for the last 15–20% of water molecules increases significantly, which is in agreement with coordination to vacant metal sites and strong hydrogen bonding to amino groups.

The apparent activation energy of the desorption reactions was calculated by the Kissinger method.[40] It is a model-free kinetic analysis, which is broadly applied for solid–gas reactions and physical interactions; see, for example, ref 41. According to Kissinger, the activation energy can be determined by applying different heating rates, via eq 2[40,41]

dx.doi.org/10.1021/cm304055k | *Chem. Mater.* 2013, 25, 790–798

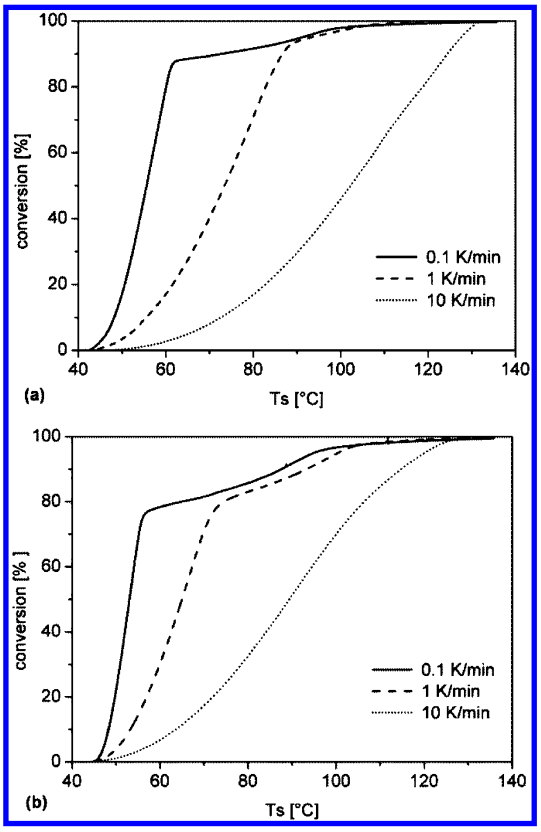

Figure 8. Desorption kinetics of (a) **1** and (b) **2** at different heating rates (Ts = sample temperature).

$$\frac{\mathrm{d}\ln\frac{\beta}{T_{\max}^{2}}}{\mathrm{d}\frac{1}{T}} = -\frac{E_a}{R} \qquad (2)$$

where β = heating rate, T_{max} = temperature at maximum rate, T = temperature, E_a = apparent activation energy, and R = gas constant. Plotting ln (β/T_{max}^2) versus $1000/RT_{max}$ gives $-E_a$ (cf. Figure 9).

In Figure 9 the values for the apparent activation energies of **1** and **2** are given. Since the standard deviation for **2** is quite high, this value serves only as orientation. The range of 91−111 kJ/mol is in fact similar to other sorption materials that work in a similar temperature−vapor pressure range: The dehydration

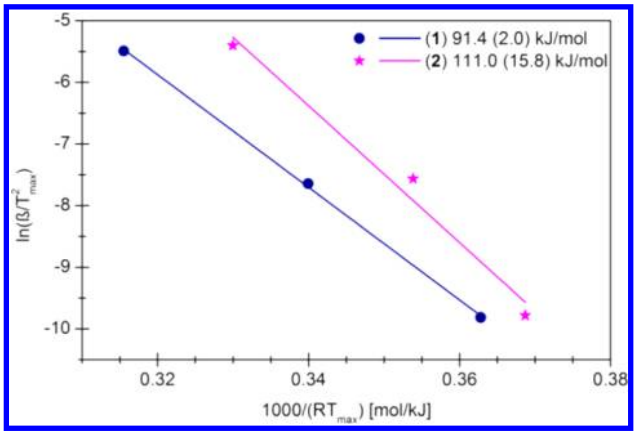

Figure 9. Kissinger plot[40] for calculation of activation energy (cf. eq 2).

of $MgCl_2{\cdot}6H_2O$ to $MgCl_2{\cdot}4H_2O$ has an activation energy of 98.3 kJ/mol, and $MgCl_2{\cdot}4H_2O$ to $MgCl_2{\cdot}2H_2O$ has an activation energy of 100.9 kJ/mol.[42] Despite the importance of kinetic data, there is a lack of activation parameters and other kinetic information about MOFs. Further research is needed in this field.

CONCLUSION

The water sorption properties of functionalized MIL-101Cr materials **1**−**4** have been investigated in order to contribute to the understanding of sorption properties as a function of functional groups. We have shown that the hydrophilic aminated materials **1** and **2** have a high recyclable water sorption capacity and start with their large water uptake earlier than nonmodified MIL-101Cr. Materials **1** and **2** exhibit no detectable loss of crystallinity or surface area; that is, they show high cycle stability. By comparison, the partially aminated compound **2** shows the best water loading for 40 subsequent water sorption cycles according to mass and enthalpy measurements. The decrease of the water uptake capacity together with BET surface and pore volume of nitro-functionalized MOFs **3** and **4** is reasoned to be due to the electron-withdrawing character and its decrease on the Cr−carboxylate bond inertness. Water desorption from **1** and **2** occurs at 55 °C for a water vapor partial pressure of 5.2 kPa but can be delayed to higher temperature by fast overheating. Activation energies for water desorption from **1** and **2** lie in the range for dehydration of ionic salts.

EXPERIMENTAL SECTION

Water cycle measurements: A Mettler Toledo TGA/DSC1 was used for the synchronized thermogravimetric analysis (TGA) and dynamic differential calorimetry (DSC) of the desorption and adsorption cycles. The TGA/DSC was coupled with a humidity generator MHG-32 from the company Projekt Messtechnik. Humidity was directly measured in the TG oven. The air humidity generator regulated the water vapor partial pressure over the full cycle to 5.2 kPa water. The TG oven was flushed with a dry nitrogen flow of 20 mL/min and a humidified nitrogen flow of 190 mL/min. A temperature cycle began after an isotherm at 40 °C for 15 min with a heating rate of 10 K/min to 140 °C, followed by an isotherm for 30 min. Then the sample was cooled again to 40 °C at a rate of 10 K/min, followed by an isotherm for 165 min. In total, 40 cycles were measured for each sample. For each sample a mass of 10−50 mg was used. The Mettler-Toledo software STARe 11.00a was used for data evaluation.

ASSOCIATED CONTENT

Supporting Information

Additional text and 19 figures giving synthesis procedures, descriptions of analytic methods, nitrogen and water sorption isotherms, and changes of absolute masses and absolute desorption enthalpy during water sorption cycle measurements (PDF). This material is available free of charge via the Internet at http://pubs.acs.org.

AUTHOR INFORMATION

Corresponding Author

*E-mail thomas.schmidt@inkubator.leuphana.de (T.S.), janiak@uni-duesseldorf.de (C.J.).

Notes

The authors declare no competing financial interest.

■ ACKNOWLEDGMENTS

Funding by the Federal German Ministry of Economics (BMWi) under Grant 0327851A/B for the work of S.H. and C.J. is gratefully acknowledged. H.U.R. thanks the Friedrich-Ebert-Stiftung for financial support. T.S. gratefully acknowledges financial support from the European Union and the Federal State of Lower Saxony.

■ ABBREVIATIONS

BET, Brunauer−Emmett−Teller; MIL, Materials Institute Lavoisier; MOF, metal−organic framework; PXRD, powder X-ray diffraction

■ REFERENCES

(1) (a) Aristov, Yu. I. *Appl. Therm. Eng.* **2013**, *50*, 1610−1618. (b) Hauer, A. *Adsorption* **2007**, *13*, 399−405. (c) Núñez, T.; Mittelbach, W.; Henning, H.-M. *Appl. Therm. Eng.* **2007**, *27*, 2205−2212. (d) Aristov, Yu. I. *J. Chem. Eng. Jpn.* **2007**, *40*, 1241−1251.

(2) (a) Demira, H.; Mobedi, M.; Ülkü, S. *Renewable Sustainable Energy Rev.* **2008**, *12*, 2381−2403. (b) Henninger, S. K.; Schmidt, F. P.; Henning, H.-M. *Appl. Therm. Eng.* **2010**, *30*, 1692−1702. (c) Henning, H.-M. *Appl. Therm. Eng.* **2007**, *27*, 1734−1749. (d) Aristov, Yu. I. *Int. J. Heat Mass Transfer* **2008**, *51*, 4966−4972. (e) Henninger, S. K.; Jeremias, F.; Kummer, H.; Schossig, P.; Henning, H.-M. *Energy Proc.* **2012**, *30*, 279−288.

(3) (a) Aristov, Yu. I. *Int. J. Refrig.* **2009**, *32*, 675−686. (b) Saha, B. B.; Jribi, S.; Koyama, S.; Aristov, Yu. I. *Int. J. Heat Mass Transfer* **2009**, *52*, 516−524. (c) Critoph, R. E.; Tamainot-Telto, Z.; Metcalf, S. J. *Int. J. Refrig.* **2009**, *32*, 1212−1229. (d) Veselovskaya, J. V.; Critoph, R. E.; Thorpe, R. N. *Appl. Therm. Eng.* **2010**, *30*, 1188−1192.

(4) Ng, E.-P.; Mintova, S. *Microporous Mesoporous Mater.* **2008**, *114*, 1−26.

(5) Seo, Y.-K.; Yoon, J. W.; Lee, J. S.; Hwang, Y. K.; Jun, C.-H.; Chang, J.-S.; Wuttke, S.; Bazin, P.; Vimont, A.; Daturi, M.; Bourrelly, S.; Llewellyn, P. L.; Horcajada, P.; Serre, C.; Férey, G. *Adv. Mater.* **2012**, *24*, 806−810.

(6) (a) Henninger, S. K.; Munz, G.; Ratzsch, K.-F.; Schossig, P. *Renewable Energy* **2011**, *36*, 3043−3049. (b) Henninger, S. K.; Schmidt, F.; Henning, H.-M. *Adsorption* **2011**, *17*, 833−843.

(7) Henninger, S. K.; Jeremias, F.; Kummer, H.; Janiak, C. *Eur. J. Inorg. Chem.* **2012**, 2625−2634.

(8) (a) Aristov, Yu. I. *Appl. Therm. Eng.* **2012**, *42*, 18−24. (b) Saha, B. B.; Chakraborty, A.; Koyama, S.; Srinivasan, K.; Ng, K. C.; Kashiwagi, T.; Dutta, P. *Appl. Phys. Lett.* **2007**, *91*, No. 111902.

(9) (a) Kitagawa, S.; Matsuda, R. *Coord. Chem. Rev.* **2007**, *251*, 2490−2509. (b) Maji, T. K.; Kitagawa, S. *Pure Appl. Chem.* **2007**, *79*, 2155−2177.

(10) (a) Zhou, H.-C.; Long, J. R.; Yaghi, O. M. *Chem. Rev.* **2012**, *112*, 673−674. (b) Stock, N.; Biswas, S. *Chem. Rev.* **2012**, *112*, 933−969. (c) Shekhah, O.; Liu, J.; Fischer, R. A.; Wöll, C. *Chem. Soc. Rev.* **2011**, *40*, 1081−1106. (d) Janiak, C.; Vieth, J. K. *New. J. Chem.* **2010**, *34*, 2366−2388. (e) Long, J. R.; Yaghi, O. M. *Chem. Soc. Rev.* **2009**, *38*, 1213−1214. (f) Czaja, A. U.; Trukhan, N.; Müller, U. *Chem. Soc. Rev.* **2009**, *38*, 1284−1293. (g) Janiak, C. *Dalton Trans.* **2003**, 2781−2804.

(11) (a) Suh, M. P.; Park, H. J.; Prasad, T. K.; Lim, D.-W. *Chem. Rev.* **2012**, *112*, 782−835. (b) Getman, R. B.; Bae, Y.-S.; Wilmer, C. E.; Snurr, R. Q. *Chem. Rev.* **2012**, *112*, 703−723. (c) Murray, L. J.; Dinca, M.; Long, J. R. *Chem. Soc. Rev.* **2009**, *38*, 1294−1314. (d) Li, J.-R.; Kuppler, R. J.; Zhou, H.-C. *Chem. Soc. Rev.* **2009**, *38*, 1477−1504. (e) Düren, T.; Bae, Y.-S.; Snurr, R. Q. *Chem. Soc. Rev.* **2009**, *38*, 1237−1247. (f) Han, S. S.; Mendoza-Cortés, J. L.; Goddard, W. A., III. *Chem. Soc. Rev.* **2009**, *38*, 1460−1476. (g) Morris, R. E.; Wheatley, P. S. *Angew. Chem., Int. Ed.* **2008**, *47*, 4966−4981. (h) Suh, M. P.; Cheon, Y. E.; Lee, E. Y. *Coord. Chem. Rev.* **2008**, *252*, 1007−1026. (i) Kepert, C. J. *Chem. Commun.* **2006**, 695−700.

(12) (a) Zhang, Z.; Zhao, Y.; Gong, Q.; Li, Z.; Li, J. *Chem. Commun.* **2013**, *49*, 653−661. (b) Tanh Jeazet, H. B.; Staudt, C.; Janiak, C. *Dalton Trans.* **2012**, *41*, 14003−14027. (c) Hunger, K.; Schmeling, N.; Tanh Jeazet, H. B.; Janiak, C.; Staudt, C.; Kleinermanns, K. *Membranes* **2012**, *2*, 727−763. (d) Tanh Jeazet, H. B.; Staudt, C.; Janiak, C. *Chem. Commun.* **2012**, *48*, 2140−2142. (e) Li, J.-R.; Sculley, J.; Zhou, H.-C. *Chem. Rev.* **2012**, *112*, 869−932. (f) Li, J.-R.; Ma, Y.; McCarthy, M. C.; Sculley, J.; Yu, J.; Jeong, H.-K.; Balbuena, P. B.; Zhou, H.-C. *Coord. Chem. Rev.* **2011**, *255*, 1791−1823. (g) Fischer, M.; Sartor, M.; Fröba, M. *Nachr. Chem.* **2010**, *58*, 1003−1007. (h) Ma, S.; Sun, D.; Ambrogio, M.; Fillinger, J. A.; Parkin, S.; Zhou, H. C. *J. Am. Chem. Soc.* **2007**, *129*, 1858−1859.

(13) Reboul, J.; Furukawa, S.; Horike, N.; Tsotsalas, M.; Hirai, K.; Uehara, H.; Kondo, M.; Louvain, N.; Sakata, O.; Kitagawa, S. *Nat. Mater.* **2012**, *11*, 717−723.

(14) (a) Wu, H. H.; Gong, Q. H.; Olson, D. H.; Li, J. *Chem. Rev.* **2012**, *112*, 836−868. (b) Nijem, N.; Wu, H. H.; Canepa, P.; Marti, A.; Balkus, K. J., Jr.; Thonhauser, T.; Li, J.; Chabal, Y. J. *J. Am. Chem. Soc.* **2012**, *134*, 15201−15204. (c) Li, K. H.; Olson, D. H.; Li, J. *Trends Inorg. Chem.* **2010**, *12*, 13−24.

(15) (a) Horcajada, P.; Gref, R.; Baati, T.; Allan, P. K.; Maurin, G.; Couvreur, P.; Férey, G.; Morris, R. E.; Serre, C. *Chem. Rev.* **2012**, *112*, 1232−1268. (b) Lohe, M. R.; Gedrich, K.; Freudenberg, T.; Kockrick, E.; Dellmann, T.; Kaskel, S. *Chem. Commun.* **2011**, *47*, 3075−3077. (c) Férey, G. *Chem. Soc. Rev.* **2008**, *37*, 191−214.

(16) (a) Bétard, A.; Fischer, R. A. *Chem. Rev.* **2012**, *112*, 1055−1083. (b) Takashima, Y.; Martínez, V. M.; Furukawa, S.; Kondo, M.; Shimomura, S.; Uehara, H.; Nakahama, M.; Sugimoto, K.; Kitagawa, S. *Nat. Commun* **2011**, *2*, 168 ; DOI: DOI: 10.1038/ncomms1170. (c) Halder, G. J.; Kepert, C. J.; Moubaraki, B.; Murray, K. S.; Cashion, J. D. *Science* **2002**, *298*, 1762−1765.

(17) (a) Yoon, M.; Srirambalaji, R.; Kim, K. *Chem. Rev.* **2012**, *112*, 1196−1231. (b) Lee, J .-Y.; Farha, O. K.; Roberts, J.; Scheidt, K. A.; Nguyen, S. T.; Hupp, J. T. *Chem. Soc. Rev.* **2009**, *38*, 1450−1459. (c) Ma, L.; Abney, C.; Lin, W. *Chem. Soc. Rev.* **2009**, *38*, 1248−1256. (d) Farrusseng, D.; Aguado, S.; Pinel, C. *Angew. Chem., Int. Ed.* **2009**, *48*, 7502−7513.

(18) (a) Meilikhov, M.; Yusenko, K.; Esken, D.; Turner, S.; Van Tendeloo, G.; Fischer, R. A. *Eur. J. Inorg. Chem.* **2010**, 3701−3714. (b) Falcaro, P.; Hill, A. J.; Nairn, K. M.; Jasieniak, J.; Mardel, J. I.; Bastow, T. J.; Mayo, S. C.; Gimona, M.; Gomez, D.; Whitfield, H. J.; Riccò, R.; Patelli, A.; Marmiroli, B.; Amenitsch, H.; Colson, T.; Villanova, L.; Buso, D. *Nat. Commun.* **2011**, *2*, 237 ; DOI: DOI: 10.1038/ncomms1234.

(19) Uemura, T.; Yanai, N.; Kitagawa, S. *Chem. Soc. Rev.* **2009**, *38*, 1228−1236.

(20) (a) Cui, Y.; Yue, Y.; Qian, G.; Chen, B. *Chem. Rev.* **2012**, *112*, 1126−1162. (b) Allendorf, M. D.; Bauer, C. A.; Bhakta, R. K.; Houk, R. J. T. *Chem. Soc. Rev.* **2009**, *38*, 1330−1352.

(21) (a) Wang, C.; Zhang, T.; Lin, W. *Chem. Rev.* **2012**, *112*, 1084−1104. (b) Evans, O. R.; Lin, W. *Acc. Chem. Res.* **2002**, *35*, 511−522.

(22) Doherty, C. M.; Knystautas, E.; Buso, D.; Villanova, L.; Konstas, K.; Hill, A. J.; Takahashif, M.; Falcaro, P. *J. Mater. Chem.* **2012**, *22*, 11470−11474.

(23) (a) Kurmoo, M. *Chem. Soc. Rev.* **2009**, *38*, 1353−1379. (b) Gil-Hernández, B.; Gili, P.; Vieth, J. K.; Janiak, C.; Sanchiz, J. *Inorg. Chem.* **2010**, *49*, 7478−7490. (c) Gil-Hernández, B.; Maclaren, J. K.; Höppe, H. A.; Pasan, J.; Sanchiz, J.; Janiak, C. *CrystEngComm* **2012**, *14*, 2635−2644.

(24) Furukawa, H.; Ko, N.; Go, Y. B.; Aratani, N.; Choi, S. B.; Choi, E.; Yazaydin, A. Ö.; Snurr, R. Q.; ÓKeeffe, M.; Kim, J.; Yaghi, O. M. *Science* **2010**, *329*, 424−428.

(25) Farha, O. K.; Yazaydın, A. Ö.; Eryazici, I.; Malliakas, C. D.; Hauser, B. G.; Kanatzidis, M. G.; Nguyen, S. T.; Snurr, R. Q.; Hupp, J. T. *Nat. Chem.* **2010**, *2*, 944−948.

(26) (a) Cohen, S. M. *Chem. Sci.* **2010**, *1*, 32−36. (b) Cohen, S. M. *Chem. Rev.* **2012**, *112*, 970−1000.

(27) Férey, G. *Dalton Trans.* **2009**, 4400−4415.

(28) Férey, G.; Serre, C. *Chem. Soc. Rev.* **2009**, *38*, 1380−1399.

(29) Henninger, S. K.; Habib, H. A.; Janiak, C. *J. Am. Chem. Soc.* **2009**, *131*, 2776−2777.

(30) Ehrenmann, J.; Henninger, S. K.; Janiak, C. *Eur. J. Inorg. Chem.* **2011**, 471−474.
(31) Küsgens, P.; Rose, M.; Senkovska, I.; Fröde, H.; Henschel, A.; Siegle, S.; Kaskel, S. *Microporous Mesoporous Mater.* **2009**, *120*, 325−330.
(32) Akiyama, G.; Matsuda, R.; Kitagawa, S. *Chem. Lett.* **2010**, *39*, 360−361.
(33) Jeremias, F.; Khutia, A.; Henninger, S. K.; Janiak, C. *J. Mater. Chem.* **2012**, *22*, 10148−10151.
(34) Férey, G.; Mellot-Draznieks, C.; Serre, C.; Millange, F.; Dutour, J.; Surblé, S.; Margiolaki, I. *Science* **2005**, *309*, 2040−2042.
(35) (a) Kim, M.; Cohen, S. M. *CrystEngComm* **2012**, *14*, 4096−4104. (b) Nguyen, H. G. T.; Weston, M. H.; Farha, O. K.; Hupp, J. T.; Nguyen, S. T. *CrystEngComm* **2012**, *14*, 4115−4118. (c) Sen Gupta, A.; Deshpande, R. K.; Liu, L.; Waterhouse, G. I. N.; Telfer, S. G. *CrystEngComm.* **2012**, *14*, 5701−5704. (d) Goesten, M. G.; Sai Sankar Gupta, K. B.; Ramos-Fernandez, E. V.; Khajavi, H.; Gascon, J.; Kapteijn, F. *CrystEngComm* **2012**, *14*, 4109−4111.
(36) Bernt, S.; Guillerm, V.; Serre, C.; Stock, N. *Chem. Commun.* **2011**, *47*, 2838−2840.
(37) Akiyama, G.; Matsuda, R.; Sato, H.; Hori, A.; Takata, M.; Kitagawa, S. *Microporous Mesoporous Mater.* **2012**, *157*, 89−93.
(38) (a) Schoenecker, P. M.; Carson, C. G.; Jasuja, H.; Flemming, C. J. J.; Walton, K. S. *Ind. Eng. Chem. Res.* **2012**, *51*, 6513−6519. (b) Cmarik, G. E.; Kim, M.; Cohen, S. M.; Walton, K. S. *Langmuir* **2012**, *28*, 15606−15613. (c) Jasuja, H.; Zang, J.; Sholl, D. S.; Walton, K. S. *J. Phys. Chem. C* **2012**, *116*, 23526−23532.
(39) Rouquerol, F.; Rouquerol, J.; Sing, K., *Adsorption by powders and porous solids*; Rouquerol, F., Rouquerol, J., Sing, K., Eds.; Academic Press: San Diego, CA, 1999; Vol. *11*.
(40) Kissinger, H. E. *Anal. Chem.* **1957**, *29*, 1702−1706.
(41) Fichtner, M.; Zhao-Karger, Z.; Hu, J.; Roth, A.; Weidler, P. *Nanotechnology* **2009**, *20*, No. 204029.
(42) Rammelberg, H. U.; Korhammer, K.; Schmidt, T.; Ruck, W. K. L. Thermodynamic and kinetic aspects of dehydration and rehydration of inorganic salt hydrates. Presented at the Wöhler-Conference 2012 in Göttingen, Germany.